


Cite this: *Nanoscale Adv.*, 2020, 2, 2531

Co-Modification of commercial TiO₂ anode by combining a solid electrolyte with pitch-derived carbon to boost cyclability and rate capabilities†

Ling-Yun Kong,^a Jing An,^a Shu-Xian Kang,^a Meng Huang,^a Huan Yang,^a Hui-Ling Zhu,^b Yong-Xin Qi,^a Xue Bai,^b Ning Lun^{*a} and Yu-Jun Bai[†]^{*a}

The bad electrochemical performance circumscribes the application of commercial TiO₂ (c-TiO₂) anodes in Li-ion batteries. Carbon coating could ameliorate the electronic conductivity of TiO₂, but the ionic conductivity is still inferior. Herein, a co-modification method was proposed by combining the solid electrolyte of lithium magnesium silicate (LMS) with pitch-derived carbon to concurrently meliorate the electronic and ionic conductivities of c-TiO₂. The homogeneous mixtures were heated at 750 °C, and the co-modified product with suitable amounts of LMS and carbon demonstrates cycling capacities of 256.8, 220.4, 195.9, 176.4, and 152.0 mA h g⁻¹ with multiplying current density from 100 to 1600 mA g⁻¹. Even after 1000 cycles at 500 mA g⁻¹, the maintained reversible capacity was 244.8 mA h g⁻¹. The superior rate performance and cyclability correlate closely with the uniform thin N-doped carbon layers on the surface of c-TiO₂ particles to favor the electrical conduction, and with the ion channels in LMS as well as the cation exchangeability of LMS to facilitate the Li⁺ transfer between the electrolyte, carbon layers, and TiO₂ particles. The marginal amount of fluoride in LMS also contributes to the excellent cycling stability of the co-modified c-TiO₂.

Received 7th March 2020
Accepted 15th April 2020

DOI: 10.1039/d0na00192a

rsc.li/nanoscale-advances

1. Introduction

The lithium-ion battery (LIB) as an energy storage system exhibits both high energy density and high safety. Nevertheless, the commercial LIBs with graphite anode cannot completely meet the requirements of the advanced energy storage systems owing to the poor rate capability and cyclability. Therefore, it is essential to explore suitable anode materials for large LIBs, especially when used in electric vehicles, grids, *etc.*

Among the varieties of anode materials, TiO₂ has been deemed to be one of the candidates on account of its outstanding cyclic reversibility with an inappreciable volume expansion (*ca.* 4%), high rate capability, and safety, especially the advantages for commercial TiO₂ (c-TiO₂) lie in the abundance, low cost, and environmental benignancy. However, the main drawbacks are the poor electronic conductivity and low Li-ion mobility as a result of the large band-gap and high energy barrier for Li-ion diffusion.¹ Several strategies have been

adopted to tackle these issues. Carbon coating is an effective method to enhance storage capacity and electrochemical kinetics.^{2–4} Among the carbon precursors, pitch as a typical soft carbon (SC) source could be readily pyrolyzed into carbon with a high graphitization degree, and the electrode materials coated with SC reveal enhanced conductivity.^{5–7} Additionally, the low softening temperature of the coal tar pitch makes it easy to create a carbon coating on metal oxides.⁸ However, the anatase TiO₂ anode coated with the SC derived from pitch revealed a capacity retention (CR) of only 48.7% after 1000 cycles at a current rate of 0.5 A g⁻¹,⁹ possibly because of the poor rate performance resulting from the sluggish Li-ion diffusion in the carbon materials.^{10–12}

In contrast to the excellent electronic conductivity, the Li-ion diffusion of carbon materials is inferior, and hence, the Li⁺ conductivity of the carbon-coated TiO₂ anode is poor. Nevertheless, solid Li-ion conductors facilitate Li⁺ diffusion. For example, the Ti-based oxide anodes modified by Li_{1.3}Al_{0.3}-Ti_{1.7}(PO₄)₃,¹³ Li₂SiO₃,¹⁴ Li₂ZrO₃,¹⁵ and LiNaAl₂₂O₃₄ (ref. 16) exhibited both outstanding rate capabilities and remarkable cycling stability. Despite the good ionic conductivity, the electron conductivity of these conductors is poor. If a hybrid material containing both carbon and an appropriate amount of solid electrolyte is employed to concurrently modify the c-TiO₂, it is expected to achieve an optimized electrochemical performance, just like what happened for the LiFePO₄ co-modified by LaPO₄ and carbon.¹⁷

^aKey Laboratory of Liquid-Solid Structural Evolution & Processing of Materials, Ministry of Education, Shandong University, Jinan 250061, PR China. E-mail: byj97@sdu.edu.cn; lunning66@sdu.edu.cn; Fax: +86 531 88392315; Tel: +86 531 88392315

^bSchool of Materials Science and Engineering, Shandong University of Science and Technology, Qingdao, 266590, PR China

† Electronic supplementary information (ESI) available. See DOI: 10.1039/d0na00192a



Lithium magnesium silicate (LMS) with good absorbability and cation exchangeability demonstrates Li-ion transport rate over 95% in a composited electrolyte and an electrical conductivity of $2 \times 10^{-4} \text{ S cm}^{-1}$ at ambient temperature.^{18,19} Furthermore, LMS is apt to coat on the surface of oxides in the sol state. The Ti-based oxide anodes of $\text{Li}_4\text{Ti}_5\text{O}_{12}$ (ref. 20) and $\text{Li}_2\text{ZnTi}_3\text{O}_8$ (ref. 21) modified by LMS demonstrated greatly enhanced performance.

In view of the above analysis, in this work, c-TiO₂ was co-modified by combining the solid electrolyte of LMS with the pitch-derived carbon to concurrently ameliorate the electronic and ionic conductivities of c-TiO₂ so as to optimize the electrochemical performance. The modification mechanism is discussed by virtue of diverse characterization methods.

2. Experimental section

2.1 Preparation of materials

c-TiO₂ was purchased from Panzhihua TaiDu Chemical Industry Co. Ltd. The ingredients of LMS was provided by the manufacturer: 55–57 wt% SiO₂, 23.5–25.0 wt% MgO, 2.8–3.8 wt% Na₂O, 1.2–1.5 wt% Li₂O, 5–5.8 wt% F. N-Methyl-2-pyrrolidone (NMP) and poly(vinylidene fluoride) (PVDF), bought from Sinopharm Chemical Reagent Co. Ltd, were of analytical grade. The electrolyte (LiPF₆ dissolved in ethyl carbonate and dimethyl carbonate in a volume ratio of 1 : 1) was purchased from Shenzhen Biyuan Electronics.

The co-modification process of c-TiO₂ by LMS and coal tar pitch is as follows. LMS was dissolved in 15 mL deionized water at 60 °C *via* magnetic stirring for 20.0 min, and then 3.5 g c-TiO₂ was added into the solution and stirred for another 10.0 min; next, 0.48 g coal tar pitch and 15 mL ethyl alcohol were dispersed in the suspension under magnetic stirring and stirred for 60.0 min. After thoroughly drying at 105 °C in air for 12 h, the mixture was heated in a tube furnace at 750 °C for 5 h in N₂ atmosphere. According to the LMS content in the mixture, the as-sintered products were labelled as TiO₂/C (0 wt% LMS), LMS1 (0.5 wt% LMS), LMS2 (1.5 wt% LMS), and LMS3 (2.4 wt% LMS).

Detailed characterization methods and electrochemical tests are supplied in the ESI.†

3. Results and discussion

3.1 Structure analysis

The microstructures of the as-prepared samples were inspected by transmission electron microscopy (TEM) (Fig. 1). After sintering at 750 °C for 5 h, the grain size of the co-modified TiO₂ was about 10–20 nm (Fig. 1a). The lattice spacing of 0.35 nm (Fig. 1b) was consistent with that of the (101) plane of anatase TiO₂, corroborating the identical anatase structure of the co-modified TiO₂. Carbon coating with one or two graphene layers was distinguished around the c-TiO₂ crystallites (Fig. 1b, d, and S1†), which linked the nanoparticles to form aggregates with a reticular structure, favorable to improve the electronic conductivity both in individual nanoparticles and among the nanoparticles. However, the coating in LMS1, LMS2, and LMS3 was somewhat different from that in TiO₂/C in terms of

graphitization degree because the presence of LMS within carbon suppresses the graphitization to a certain degree.

Little LMS was detected by TEM because of the low additive content, poor crystallization degree, and instability under the irradiation of high-energy electron beams²⁰ (Fig. 1c and S1†). To determine the presence of LMS, the microstructure of LMS3 with the highest LMS content was scrutinized, and some layered structures were detected to distribute between the TiO₂ grains or on the surface of TiO₂ particles (Fig. S1†). Though the irradiation of high-energy electron beams results in the amorphization of LMS, the metastable structure was favorable for Li-ion transfer at low temperatures. Upon combining the HAADF-STEM examination and EDS mapping of LMS2 in Fig. 1e, the distribution of Si and Mg gives further evidence for LMS around the c-TiO₂ crystallites. More microstructures are supplied in Fig. S1 of ESI.†

In the X-ray diffraction (XRD) patterns of the co-modified TiO₂ sintered at 750 °C for 5 h (Fig. 2a), the diffraction peaks pertain well to those of the anatase TiO₂ (JPCDS no. 21-1272). The average grain sizes calculated by the Scherrer equation ($D = K\lambda/\beta \cos \theta$ with K -constant, λ -wavelength of X-rays, β -full width at half maximum, and θ -Bragg angle) based on the (101) plane were about 37.5, 17.8, 17.3, 17.2, and 17.7 nm for TiO₂, TiO₂/C, LMS1, LMS2, and LMS3, respectively. Evidently, the grain growth of TiO₂ was hindered by coating carbon due to the

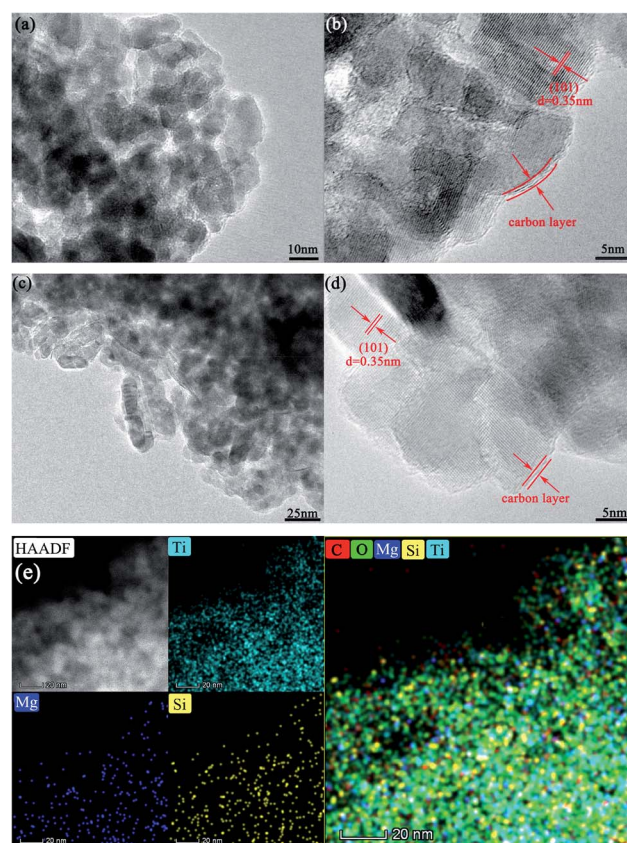


Fig. 1 The TEM images of TiO₂/C (a and b) and LMS2 (c and d). (e) The HAADF-STEM image of LMS2 and EDS mappings: Ti map, Mg map, Si map, and mixed color map of C, O, Mg, Si, and Ti.



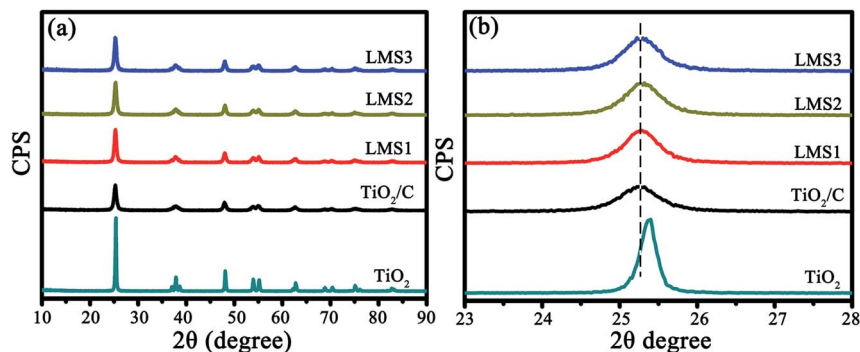


Fig. 2 The XRD patterns of TiO_2 , TiO_2/C , LMS1, LMS2, and LMS3 (a) as well as the magnified patterns for the (101) plane of TiO_2 (b).

prevention of atom diffusion and particle agglomeration. The smaller crystallite size could shorten the Li-ion diffusion distance during charging and discharging. From the enlarged (101) peaks (Fig. 2b), the analogous left shift of the diffraction angle for both the co-modified TiO_2 and TiO_2/C denotes the presence of similar element-doping in TiO_2 , as demonstrated by the X-ray photoelectron spectroscopy (XPS) analysis.

3.2 XPS

The interaction of c- TiO_2 with LMS and the carbon derived from coal tar pitch was further assessed by XPS. Taking LMS2 as an example, the elements Li, Si, Mg, N, F, Ti, and O were present in the survey spectrum (Fig. 3a), where the N element originates from the nitrogenous organic molecules in coal tar pitch (such as pyrrole)²² and the F element from LMS. The slightly asymmetric C 1s spectrum could be fitted into four peaks (Fig. 3b), *i.e.*, the characteristic C–C bonds at 284.8 eV, C=N bonds at 285.8 eV, C–O bonds at 286.8 eV, and C–F bonds at 289.0 eV. The deconvoluted F 1s spectrum (Fig. 3g) includes four components, namely C–F, Li–F, Mg–F, and Na–F at around 688.3, 686.7, 685.25, and 684.3 eV, respectively. Both the N and F-doped carbon coating will produce a positive effect on the electrochemical performance.^{23–26} The deconvolution of the Ti 2p spectrum (Fig. 3c) yields three peaks, *i.e.* peaks corresponding to Ti 2p_{3/2} at around 459.4 eV and Ti 2p_{1/2} at around 464.2 eV, and an extra peak at around 460.3 eV that stemmed from the N–Ti–O linkage, which is responsible for the augmented lattice parameters of TiO_2 in the XRD patterns.^{27–29} The N 1s spectrum could be deconvoluted into Ti–N, pyridinic-N, pyrrolic-N, and graphitic-N at around 396.2, 398.2, 400.1, and 401.6 eV, respectively³⁰ (Fig. 3h), demonstrating N-doping in both carbon and TiO_2 . Besides the Si 2p spectrum with a peak at around 103.6 eV (Fig. 3f), the fitted Li 1s spectrum contains two peaks of Li–F (55.7 eV) and Li–O (55.5 eV) (Fig. 3d) and the fitted Mg 2p spectrum consists of three peaks of Mg–F (50.9 eV), Mg–O in LMS (51.2 eV), and MgO (50.3 eV) (Fig. 3e). Apparently, the XPS spectra of LMS2 reveals the presence of Li–O, Mg–O, and Si–O bonds with their binding energies close to those in LMS (Fig. 3), providing further evidence for LMS and the composition. The N-doped TiO_2 coated with the N- and F-doped carbon contributes to enhancing the electron conduction, and the marginal

amount of fluoride was found to be favorable to boost the cycling stability of the anode materials.³¹

3.3 Thermogravimetric analysis (TGA) and Raman spectroscopy (RS)

The presence of carbon and its content were identified by TGA and RS, as exemplified by TiO_2/C and LMS2 (Fig. 4). The mass loss in the temperature ranges of 25–200, 200–500 and 500–620 °C represents the evaporation of moisture absorbed, the oxidation of amorphous carbon and graphitic carbon, respectively^{32,33} (Fig. 4a). The mass ratio for the amorphous to graphitic carbon was *ca.* 1 : 1. The carbon content was 12.6, 11.5, and 12.6 wt% for LMS1, LMS2, and LMS3, respectively. In analogy, the carbon content in TiO_2/C was 12.8 wt% (Fig. S2†).

In the Raman spectra (Fig. 4b), two characteristic bands at *ca.* 1360 (D-band) and 1590 cm^{-1} (G-band) further confirm the presence of carbon. The average intensity ratio of the two bands (I_D/I_G) was 0.935, 0.969, 0.975, and 0.967 for TiO_2/C , LMS1, LMS2, and LMS3 (Fig. 4b and S3†), respectively, signifying that the addition of LMS slightly hindered the graphitization of the pitch-derived carbon, consistent with the TEM observation.

3.4 Electrochemical performance

The electrochemical properties of the co-modified TiO_2 and TiO_2/C were evaluated by galvanostatically discharging/charging at 100 mA g^{-1} (Fig. 5a). The initial discharge/charge capacities for TiO_2/C , LMS1, LMS2, and LMS3 were 646.6/346.3, 622.3/323.8, 637.4/322.5, and 474.5/229.2 mA h g^{-1} , respectively, and the irreversible capacity stems from the creation of the SEI films and some other irreversible electrochemical reactions with the electrolyte.³⁴ After 100 cycles, TiO_2/C displayed a discharge capacity of 328.7 mA h g^{-1} , which is higher than those of LMS1 (265.2 mA h g^{-1}) and LMS2 (290.5 mA h g^{-1}). Especially, LMS3 with the highest LMS content exhibited the lowest discharge capacity of 196.9 mA h g^{-1} after 100 cycles. Thus, the addition of LMS influences the performance greatly. Moreover, despite the slight capacity decay in the initial several cycles, the coulombic efficiency approaches nearly 100% thereafter, manifesting the superior reversibility of the co-modified TiO_2 and TiO_2/C .



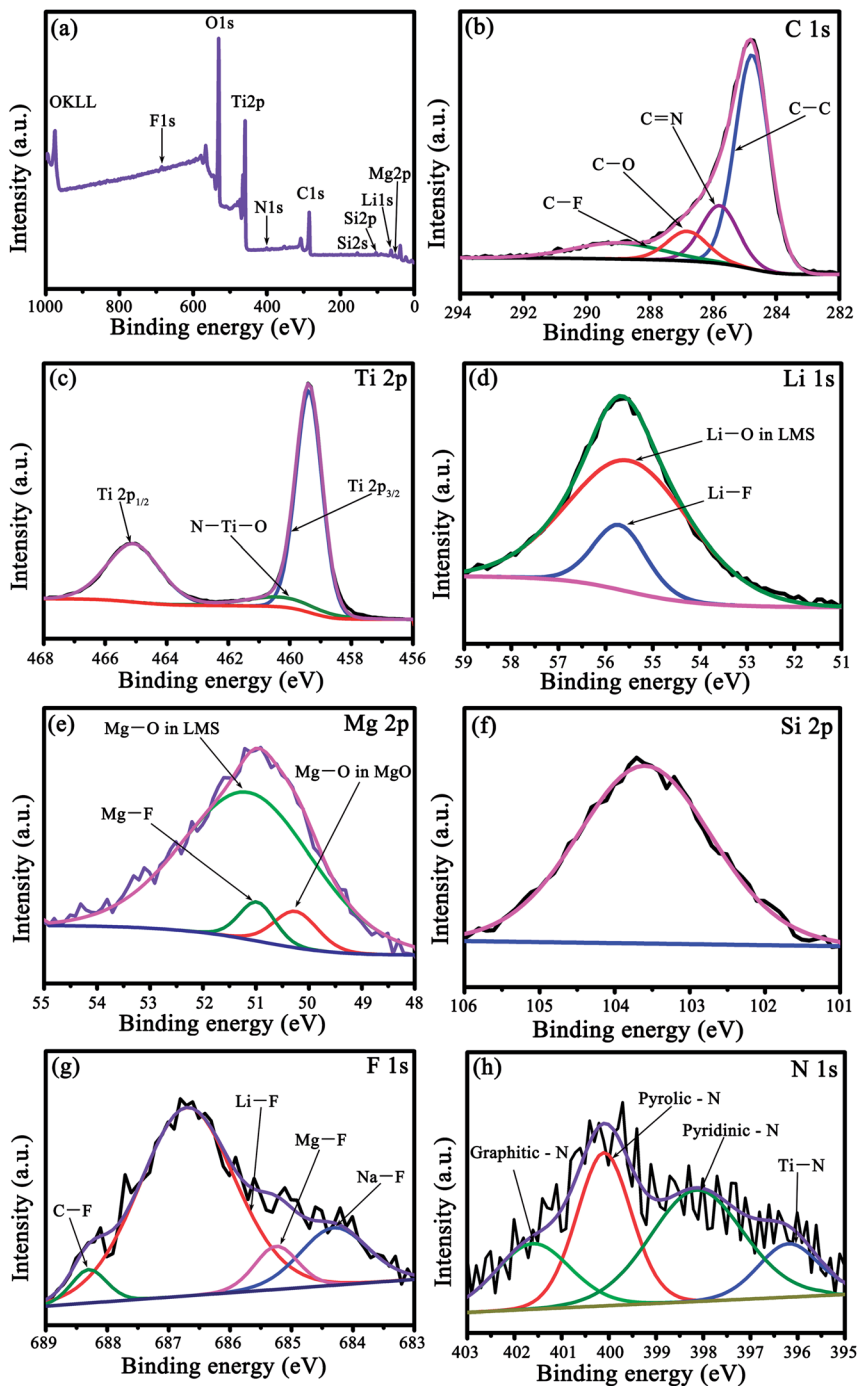


Fig. 3 The XPS spectra of LMS2. (a) The Survey spectrum, (b) C 1s, (c) Ti 2p, (d) Li 1s, (e) Mg 2p, (f) Si 2p, (g) F 1s, and (h) N 1s.

Rate capabilities were evaluated by altering the discharge/charge rate (Fig. 5b), and the mean discharge capacities and CR are collected in Table 1. Apparently, the CR of LMS1, LMS2, and LMS3 were higher than that of TiO_2/C at the corresponding current rate. Especially, the capacity of LMS2 fades slowly with an increase in the current rate, attaining the highest CR at each current rate and the highest capacity at 1600 mA g^{-1} , thereby revealing the best rate performance among the samples. In contrast, TiO_2/C and LMS3 demonstrate poor high-rate performance due to the absence of LMS and excess LMS, respectively.

The cycling stability was identified at 500 mA g^{-1} after the rate performance evaluation (Fig. 5c–e). After undergoing 1000 cycles, LMS1 and LMS3 exhibited reversible capacities of 154.3 and $187.1 \text{ mA h g}^{-1}$ with the CR of 71.4% and 100% , respectively. For TiO_2/C , the initial discharge capacity of $204.3 \text{ mA h g}^{-1}$ fades continuously to $111.7 \text{ mA h g}^{-1}$ with the CR of only 54.7% . In particular, LMS2 reveals the most preferable cyclability, achieving a discharge capacity of $244.8 \text{ mA h g}^{-1}$ after 1000 cycles with a coulombic efficiency of nearly 100% . The superior reversibility and cycling stability of the co-modified TiO_2 to TiO_2/C demonstrate



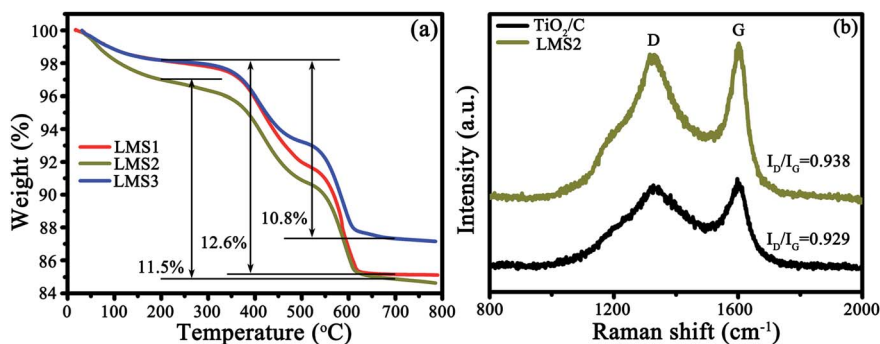


Fig. 4 TG curves (a) and RS (b) of TiO_2/C and LMS2.

the important role of LMS for the performance of TiO_2 , and the appropriate LMS content brings about the optimal performance.

The CV profiles were measured for three cycles (Fig. 6). In the 1st cycle (Fig. 6a and b), a couple of redox peaks around 1.5/2.25 V

attribute to Li^+ intercalation/deintercalation in anatase TiO_2 , *i.e.*, $\text{TiO}_2 + x\text{Li}^+ + xe \leftrightarrow \text{Li}_x\text{TiO}_2$ ($0 \leq x \leq 0.5$),^{35,36} and a weak cathodic peak at *ca.* 0.58 V correlates with the creation of the SEI films. From Fig. 6 and S4,[†] it is clear that the as-modified TiO_2 could

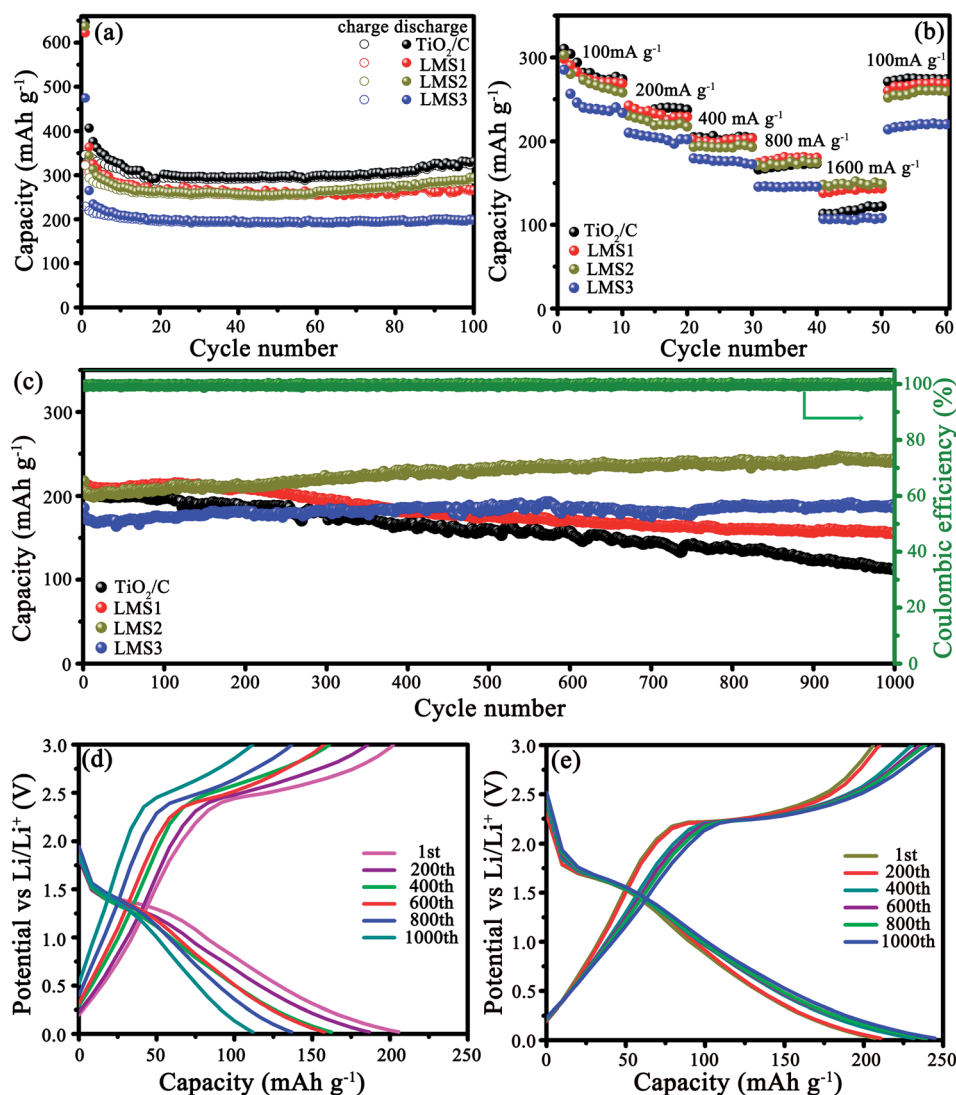


Fig. 5 Cycling property at 100 mA g^{-1} (a), rate capabilities (b), and cycling property at 500 mA g^{-1} (c) for TiO_2/C , LMS1, LMS2 and LMS3, discharge–charge curves of TiO_2/C (d) and LMS2 (e) for the selected cycles at 500 mA g^{-1} .



Table 1 Mean discharge capacities (mA h g⁻¹) and CR (%) with altering current rate (mA g⁻¹)

Sample	Capacity/CR with altering the current rate				
	100	200	400	800	1600
TiO ₂ /C	285.4/100	238.2/83.5	204.1/71.5	170.6/59.8	117.5/41.2
LSM1	277.1/100	233.1/84.1	201.0/72.5	179.1/64.6	142.0/51.2
LMS2	256.8/100	220.4/85.8	195.9/76.3	176.4/68.7	152.0/59.2
LMS3	234.0/100	204.7/86.3	176.0/75.2	145.8/62.3	108.4/46.3

store a considerable amount of Li ions below 1.0 V due to the pseudocapacitive interfacial storage effect^{37,38} and Li⁺ intercalation in carbon.^{39,40} In the 3rd cycle, the potential difference between the redox peaks were 0.7, 0.63, and 0.59 V for LMS1, LMS2, and LMS3, respectively, which is distinctly smaller than that for TiO₂/C (0.87 V), thereby denoting the alleviated polarization in the presence of LMS.⁴¹ Similar results are also reflected by the discharge–charge curves of TiO₂/C and LMS2 in Fig. 6d and e. On the contrary, both the cathodic and anodic peaks for TiO₂/C reveal poor coincidence and larger hysteresis (Fig. 6a), implying the inferior electrochemical kinetics of the samples with LMS.

The Li⁺ diffusion coefficient (D_{Li^+}) was computed by virtue of the CV data based on eqn (1).^{42,43}

$$I_p = 2.69 \times 10^5 n^{3/2} A D^{1/2} \nu^{1/2} \Delta C_0 \quad (1)$$

where, I_p is the peak current in the third CV cycle (acquired from Fig. 6), A is the surface area of the electrode (1.5386 cm²), n is

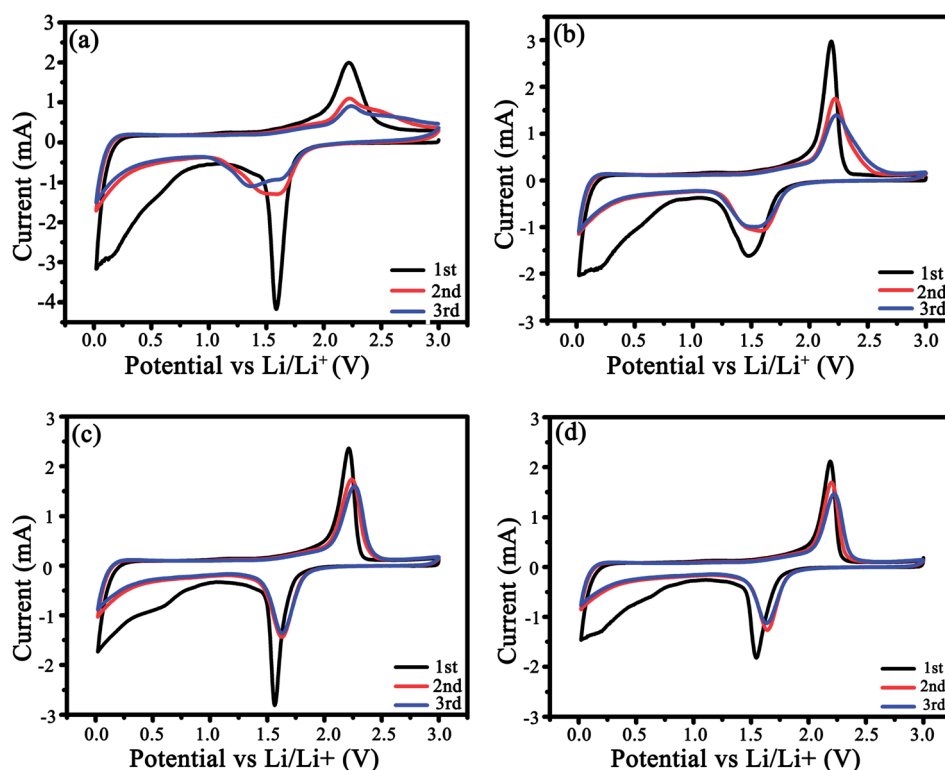
Table 2 D_{Li^+} values for TiO₂/C, LMS1, LMS2 and LMS3

Sample	I_p /mA	D_{Li^+} /cm ² s ⁻¹
TiO ₂ /C	0.906	2.82×10^{-11}
LMS1	1.398	6.71×10^{-11}
LMS2	1.600	8.80×10^{-11}
LMS3	1.467	7.39×10^{-11}

the number of electrons per molecule during oxidation ($n = 1$), ΔC_0 is the concentration of Li-ion (0.0238 mol cm⁻³), and $\nu = 0.3 \times 10^{-3}$ V s⁻¹.

The D_{Li^+} values computed by eqn (1) are tabulated in Table 2. Compared to the D_{Li^+} for TiO₂/C, the appropriate addition of LMS brings about more than three times increase in the D_{Li^+} value because of the interaction between LMS and the electrolyte. Especially, LMS2 exhibits the largest D_{Li^+} value. However, the D_{Li^+} value does not increase constantly with the increasing LMS content, just like what occurred in other modified electrode materials,^{14,20,21} because excess LMS will lead to a decrease in the electrical conductivity, thereby resulting in the mismatch between the electronic and ionic conductivities. Therefore, only the proper mass ratio of LMS/TiO₂ (say 0.015) could achieve a good match between Li⁺ diffusion and electrical conduction, contributing to the utmost optimization of the electrochemical property.

The electrochemical kinetics of the co-modified c-TiO₂ was further surveyed by EIS after three CV cycles (Fig. 7). In the Nyquist plots (Fig. 7a), the consistency of the fitting results with

**Fig. 6** CV plots of (a) TiO₂/C, (b) LMS1, (c) LMS2, and (d) LMS3 at 0.3 mV s⁻¹.

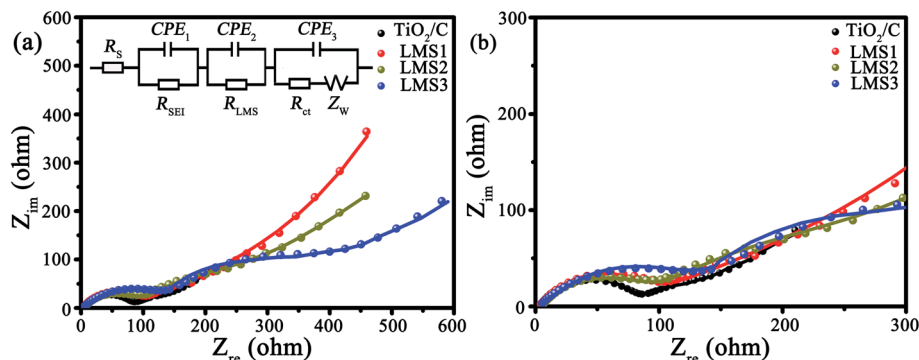


Fig. 7 (a) EIS as well as the corresponding equivalent circuit, and (b) the enlarged EIS at high frequency.

the experimental ones implies the rationality of the equivalent circuit in the inset. The impedance values of the modified TiO_2 that stemmed from the equivalent circuit are collected in Table 3, where R_s is the ohmic resistance from the electrolyte, R_{LMS} is the resistance from LMS, R_{SEI} is the resistance from the SEI films, R_{ct} is the charge transfer resistance, and Z_w is the Warburg impedance. The R_{SEI} , R_{LMS} , and R_{ct} values increase gradually with the increasing LMS content due to the poor electrical conductivity of LMS. In other words, LMS functions partially as the SEI films.

3.5 Discussion

According to the literature,⁹ when c- TiO_2 was modified by the SC derived from pitch, the performance could be greatly improved compared to the pristine c- TiO_2 . However, the capacity still faded with cycling at 500 mA g^{-1} , *i.e.* the cycling stability was unsatisfactory. Jointly adopting pitch and LMS as the modifiers brings about the distinct enhancement in the rate performance and cycling stability, where the uniform carbon layers with high graphitization degree derived from pitch favor the electron transfer among the c- TiO_2 particles (Fig. 1 and S1†), and LMS promotes the Li-ion migration in the carbon coating and c- TiO_2 (Table 2). In spite of the inferior electronic conductivity of LMS as the solid electrolyte, its high ionic conductivity contributes to the Li-ion transfer,^{14,17,20,21,44} especially making up for the deficiency of low Li-ion diffusion in the carbon materials. Only when the electronic conductivity matched well with the ionic conductivity, the electrochemical performance could be optimized as large as possible. This is the reason that LMS2 exhibits optimal performance among the samples. In addition, the N-doping in TiO_2 as well as the N- and F co-doping makes a contribution to the electrochemical performance.^{4,10,23–29,45}

Table 3 Fitted impedance for TiO_2/C , LMS1, LMS2 and LMS3

Sample	R_s/Ω	R_{SEI}/Ω	R_{LMS}/Ω	R_{ct}/Ω	R_T/Ω
TiO_2/C	2.0	42.9	—	53.1	98.0
LMS1	3.2	54.5	189.5	92.3	339.5
LMS2	3.1	75.3	267.2	102.0	447.6
LMS3	2.2	74.3	292.7	103.2	472.4

Combining the performance with the structure, microstructure, and composition, the co-modification mechanism could be briefly reflected by the illustration in Fig. 8. The N-doped carbon layers linking into a reticular structure promote the electron transfer both in the individual c- TiO_2 nanoparticles and among the nanoparticles, while LMS between the TiO_2 grains or on the surface of TiO_2 nanoparticles contributes to the Li-ion exchange not only between the electrolyte and TiO_2 nanoparticles but also among the nanoparticles.

The electrochemical performance of LMS2 was compared with that of the other carbon-coated TiO_2 reported in the literature, and is summarized in Table S1 of ESI.† Apparently, LMS2 presents much better electrochemical performances. As stated above, the excellent electrochemical performance of the carbon and LMS co-modified c- TiO_2 is related to the following aspects. (1) The coal tar pitch with excellent flow ductility could adhere uniformly on the surface of TiO_2 particles during heating and readily form uniform thin N-doped carbon layers during further carbonization at $750 \text{ }^\circ\text{C}$ to effectively ameliorate the electronic conductivity of c- TiO_2 . (2) The ion channels in LMS and the cation exchangeability of LMS promote the Li^+ transfer between the electrolyte, carbon layers, and TiO_2 particles. (3) LMS could behave as stable SEI films to prolong the cycle life of LIBs. (4) The marginal amount of fluorides in LMS was also responsible for the excellent cycling stability of the co-modified c- TiO_2 .^{46–49}

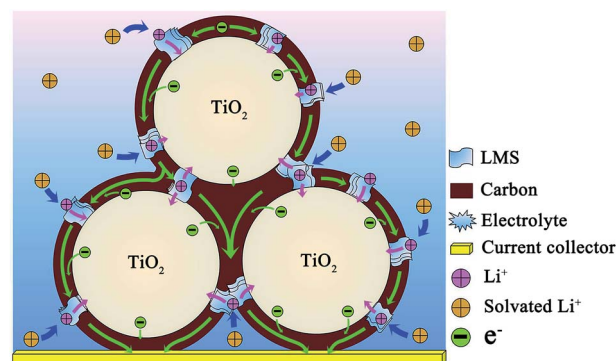


Fig. 8 Schematic illustration of co-modified TiO_2 for lithium storage processes.



4. Conclusions

In conclusion, the co-modification of c-TiO₂ by combining the solid electrolyte of LMS and pitch-derived carbon brings about the optimal performance. Besides the formation of the uniform thin N-doped carbon layers on the surface of TiO₂ particles to improve the electronic conductivity, the ion channels in LMS and the cation exchangeability of LMS facilitate the Li⁺ transfer between the electrolyte, carbon layers, and TiO₂ particles, thus realizing the simultaneous enhancement in the electrical conduction and Li-ion diffusion. Accordingly, the co-modified c-TiO₂ demonstrates excellent rate capabilities and cyclability. Therefore, the simple fabrication route and cheap modifiers, namely LMS and pitch, endow the co-modified c-TiO₂ with promising applications in advanced LIBs, especially for electric vehicles.

Conflicts of interest

There are no conflicts to declare.

Acknowledgements

This work was supported by project ZR2019MEM029 of Shandong Provincial Natural Science Foundation, PR China, and National Natural Science Foundation of China (51902189).

References

- 1 Y. Yang, X. Ji, M. Jing, H. Hou, Y. Zhu, L. Fang, X. Yang, Q. Chen and C. E. Banks, *J. Mater. Chem. A*, 2015, **3**, 5648–5655.
- 2 J. Chen, Y. Li, J. Mu, Y. Zhang, Z. Yu, K. Han and L. Zhang, *J. Alloys Compd.*, 2018, **742**, 828–834.
- 3 N. Takezawa, H. Kobayashi, M. Senna, T. Matsumoto, K. Saeki, J. Shi and N. Suzuki, *J. Phys. Chem. Solids*, 2019, **125**, 1–7.
- 4 M. Luo, X. Yu, W. Zhao, R. Xu, Y. Liu and H. Shen, *ACS Appl. Mater. Interfaces*, 2018, **10**, 35060–35068.
- 5 X.-Y. Zhao, X. Bai, W. Yang, D. Shen, H. Yang, N. Lun, Y.-X. Qi and Y.-J. Bai, *New J. Chem.*, 2016, **40**, 9986–9992.
- 6 K.-T. Kim, C.-Y. Yu, C. S. Yoon, S.-J. Kim, Y.-K. Sun and S.-T. Myung, *Nano Energy*, 2015, **12**, 725–734.
- 7 K.-T. Kim, G. Ali, K. Y. Chung, C. S. Yoon, H. Yashiro, Y.-K. Sun, J. Lu, K. Amine and S.-T. Myung, *Nano Lett.*, 2014, **14**, 416–422.
- 8 K. Wang, D. Ju, G. Xu, Y. Wang, S. Chen, J. Zhang, Y. Wu and W. Zhou, *Int. J. Hydrogen Energy*, 2019, **44**, 25199–25206.
- 9 L.-Y. Wang, X. Bai, Y. Wu, N. Lun, Y.-X. Qi and Y.-J. Bai, *Electrochim. Acta*, 2016, **212**, 155–161.
- 10 X. Li, X. Zhu, Y. Zhu, Z. Yuan, L. Si and Y. Qian, *Carbon*, 2014, **69**, 515–524.
- 11 C. Ma, X. Shao and D. Cao, *J. Mater. Chem.*, 2012, **22**, 8911–8915.
- 12 J. Zhang, Z. Yang, J. Qiu and H.-W. Lee, *J. Mater. Chem. A*, 2016, **4**, 5802–5809.
- 13 J.-P. Han, B. Zhang, L.-Y. Wang, H.-L. Zhu, Y.-X. Qi, L.-W. Yin, H. Li, N. Lun and Y.-J. Bai, *ACS Sustainable Chem. Eng.*, 2018, **6**, 7273–7282.
- 14 X. Bai, T. Li, Z. Dang, Y.-X. Qi, N. Lun and Y.-J. Bai, *ACS Appl. Mater. Interfaces*, 2017, **9**, 1426–1436.
- 15 J.-P. Han, B. Zhang, L.-Y. Wang, Y.-X. Qi, H.-L. Zhu, G.-X. Lu, L.-W. Yin, H. Li, N. Lun and Y.-J. Bai, *ACS Appl. Mater. Interfaces*, 2018, **10**, 24910–24919.
- 16 B. Zhang, J.-P. Han, L.-Y. Wang, N. Lun, H.-L. Zhu, L.-W. Yin, H. Li, Y.-X. Qi and Y.-J. Bai, *Appl. Surf. Sci.*, 2018, **447**, 279–286.
- 17 Z. Ma, Y. Peng, G. Wang, Y. Fan, J. Song, T. Liu, X. Qin and G. Shao, *Electrochim. Acta*, 2015, **156**, 77–85.
- 18 M. Riley, P. S. Fedkiw and S. A. Khan, *J. Electrochem. Soc.*, 2002, **149**, A667–A674.
- 19 R. G. Singhal, M. D. Capracotta, J. D. Martin, S. A. Khan and P. S. Fedkiw, *J. Power Sources*, 2004, **128**, 247–255.
- 20 X. Bai, B. Zhang, G.-Z. Jiang, J.-P. Han, N. Lun, Y.-X. Qi, J. Qiu, G.-X. Lu, Z. Qian and Y.-J. Bai, *Electrochim. Acta*, 2019, **295**, 891–899.
- 21 H. Yang, N. Lun, Y.-X. Qi, H.-L. Zhu, J.-R. Liu, J.-K. Feng, L.-l. Zhao and Y.-J. Bai, *Electrochim. Acta*, 2019, **315**, 24–32.
- 22 J. Alcaniz-Monge, D. Cazorla-Amoros and A. Linares-Solano, *Fuel*, 2001, **80**, 41–48.
- 23 D. Qu, X. Feng, X. Wei, L. Guo, H. Cai, H. Tang and Z. Xie, *Appl. Surf. Sci.*, 2017, **413**, 344–350.
- 24 L. Guo, H. He, Y. Ren, C. Wang and M. Li, *Chem. Eng. J.*, 2018, **335**, 32–40.
- 25 K. Meng, Q. Liu, Y. Huang and Y. Wang, *J. Mater. Chem. A*, 2015, **3**, 6873–6877.
- 26 J. Zhang, L. Qu, G. Shi, J. Liu, J. Chen and L. Dai, *Angew. Chem., Int. Ed.*, 2016, **55**, 2230–2234.
- 27 J. Yang, Z. Ju, Y. Jiang, Z. Xing, B. Xi, J. Feng and S. Xiong, *Adv. Mater.*, 2018, **30**, 1700104.
- 28 Y. Xing, S. Wang, B. Fang, G. Song, D. P. Wilkinson and S. Zhang, *J. Power Sources*, 2018, **385**, 10–17.
- 29 Y. Wu, X. Liu, Z. Yang, L. Gu and Y. Yu, *Small*, 2016, **12**, 3522–3529.
- 30 S. Akula and A. Sahu, *J. Electrochem. Soc.*, 2019, **166**, F93–F101.
- 31 Y. Ma, B. Ding, G. Ji and J. Y. Lee, *ACS Nano*, 2013, **7**, 10870–10878.
- 32 U. Lafont, L. Simonin, M. Gaberscek and E. Kelder, *J. Power Sources*, 2007, **174**, 1104–1108.
- 33 Y. Zhang, C. Wang, H. Hou, G. Zou and X. Ji, *Adv. Electron. Mater.*, 2016, **1600173**.
- 34 D. Zhou, W.-L. Song, X. Li and L.-Z. Fan, *Electrochim. Acta*, 2016, **207**, 9–15.
- 35 G. Nuspl, K. Yoshizawa and T. Yamabe, *J. Mater. Chem.*, 1997, **7**, 2529–2536.
- 36 Y. Xiao, X. Wang, Y. Xia, Y. Yao, E. Metwalli, Q. Zhang, R. Liu, B. Qiu, M. Rasool and Z. Liu, *ACS Appl. Mater. Interfaces*, 2014, **6**, 18461–18468.
- 37 Y. Liang, N. Li, F. Li, Z. Xu, Y. Hu, M. Jing, K. Teng, X. Yan and J. Shi, *Electrochim. Acta*, 2019, **279**, 1063–1070.



- 38 H. Wei, E. F. Rodriguez, A. F. Hollenkamp, A. I. Bhatt, D. Chen and R. A. Caruso, *Adv. Funct. Mater.*, 2017, **27**, 1703270.
- 39 Y. F. Yuan, F. Chen, S. M. Yin, L. N. Wang, M. Zhu, J. L. Yang, Y. C. Wu and S. Y. Guo, *J. Power Sources*, 2019, **420**, 38–45.
- 40 P. Zhang, J. Qiu, Z. Zheng, G. Liu, M. Ling, W. Martens, H. Wang, H. Zhao and S. Zhang, *Electrochim. Acta*, 2013, **104**, 41–47.
- 41 P. Wei, Y. Liu, Y. Su, L. Miao, Y. Huang, Y. Liu, Y. Qiu, Y. Li, X. Zhang and Y. Xu, *ACS Appl. Mater. Interfaces*, 2018, **11**, 3116–3124.
- 42 L.-l. Wang, P.-h. Ma, K. Zhang, C.-h. Gao and C.-y. Yan, *J. Salt Lake Res.*, 2009, **17**, 52–55.
- 43 Y. Cui, X. Zhao and R. Guo, *Electrochim. Acta*, 2010, **55**, 922–926.
- 44 C. Wang, Y. Gong, B. Liu, K. Fu, Y. Yao, E. Hitz, Y. Li, J. Dai, S. Xu and W. Luo, *Nano Lett.*, 2016, **17**, 565–571.
- 45 M. Ren, H. Xu, F. Li, W. Liu, C. Gao, L. Su, G. Li and J. Hei, *J. Power Sources*, 2017, **353**, 237–244.
- 46 M. Xia, Y.-r. Li, Y.-f. Wu, H.-b. Zhang, J.-k. Yang, N. Zhou, Z. Zhou and X. Xiong, *Appl. Surf. Sci.*, 2019, **480**, 410–418.
- 47 Y. Yang, Z. Wang, G. Yan, H. Guo, J. Wang, X. Li, Y. Zhou and R. Zhou, *Ceram. Int.*, 2017, **43**, 8590–8595.
- 48 S. Choudhury and L. A. Archer, *Adv. Electron. Mater.*, 2016, **2**, 1500246.
- 49 M. Haruta, Y. Kijima, R. Hioki, T. Doi and M. Inaba, *Nanoscale*, 2018, **10**, 17257–17264.

